# Variation and Interaction of Distinct Subgenomes Contribute to Growth Diversity in Intergeneric Hybrid Fish

Li Ren[1,#], Mengxue Luo[1,#], Jialin Cui[1], Xin Gao[1], Hong Zhang[1], Ping Wu[1], Zehong Wei[1], Yakui Tai[1], Mengdan Li[1], Kaikun Luo[1], Shaojun Liu[1,2,*]

[1] *State Key Laboratory of Developmental Biology of Freshwater Fish, Engineering Research Center of Polyploid Fish Reproduction and Breeding of the State Education Ministry, College of Life Sciences, Hunan Normal University, Changsha 410081, China*

[2] *Guangdong Laboratory for Lingnan Modern Agriculture, South China Agricultural University, Guangzhou 510642, China*

[#] Equal contribution.

[*] Corresponding author.

E-mail: lsj@hunnu.edu.cn (Liu S).

**Running title:** *Ren L et al / Variation and Interaction of Subgenomes in Hybrid*

The count of words: 7390.

The count of references: 50.

The count of figures: 6.

The count of supplementary figures: 7.

The count of supplementary tables: 11.

The count of letters in the article title: 94.

The count of KEYWORDS: 5.

The count of words in Abstract: 235.

## Abstract

Intergeneric hybridization greatly reshapes regulatory interactions among allelic and non-allelic genes. However, their effects on growth diversity remain poorly understood in animals. In this study, we conducted whole-genome sequencing and RNA sequencing (RNA-seq) analyses in diverse hybrid varieties resulting from the intergeneric hybridization of goldfish (*Carassius auratus* red var.) and common carp (*Cyprinus carpio*). These hybrid individuals were characterized by distinct mitochondrial genomes and copy number variations. Through a weighted gene correlation network analysis, we identified 3693 genes as candidate growth-regulated genes. Among them, the expression of 3672 genes in subgenome R (originating from goldfish) displayed negative correlations with growth rate, whereas 20 genes in subgenome C (originating from common carp) exhibited positive correlations. Notably, we observed intriguing patterns in the expression of *slc2a12* in subgenome C, showing opposite correlations with body weight that changed with water temperatures, suggesting differential interactions between feeding activity and weight gain in response to seasonal changes for hybrid animals. In 40.31% of alleles, we observed dominant *trans*-regulatory effects in the regulatory interaction between distinct alleles from subgenomes R and C. Integrating analyses of allelic-specific expression and DNA methylation data revealed that the influence of DNA methylation on both subgenomes shapes the relative contribution of allelic expression to the growth rate. These findings provide novel insights into the interaction of distinct subgenomes that underlie heterosis in growth traits and contribute to a better understanding of multiple allele traits in animals.



**KEYWORDS:** Intergeneric hybridization; Distinct allelic regulation; Growth diversity; Copy number variations; Mitochondrial regulation

## Introduction

Hybridization and polyploidization could rapidly shape various genotypes and phenotypes, providing us with abundant materials for studying the contribution of genetic regulation to phenotypes [1]. Interspecific hybridization in some plants, including *Triticum aestivum* × *Secale cereal* [2] and *Brassica nigra* × *Brassica rapa* [3], is always used to obtain varieties with excellent economic traits. In fish breeding, interspecific hybridization involving different genera or subfamilies has been detected in cyprinid fish [4,5], salmonid fish [6], and cichlid fish [7]. Among these fishes, *Cyprinus carpio* (common carp) and *Carassius auratus* red var. (goldfish) shared a common whole genome duplication (WGD) event [13.75 million years ago (Mya)] as different genera of the subfamily Cyprinidae and then diverged at 10.0 Mya [8]. The specific WGD results in bigger genome sizes and more chromosome numbers (2n: 100) in them than in most carp [9]. Recent studies show that the high genome plasticity and diverse allelic expression shape distinct morphological characters (*e.g.*, body size and color) in some varieties of them, including goldfish and koi carp [10,11]. Meanwhile, these characteristics contribute to their adaptability in the diverse environment of slow-moving rivers, lakes, and ponds [10–13]. Interesting, a nascent allopolyploid lineage ($4nR_2C_2$, $F_3$–$F_{28}$) was successfully established by the hybridization of female goldfish and male common carp and subsequent WGD [5,14]. Gene conversion, accompanied by allopolyploidization and multigenerational inheritance, resulted in the emergence of diverse growth phenotypes in the allopolyploid progenies [15,16].

Body growth, a classic quantitative trait that includes height in humans and weight in domestic animals [17,18], exhibits significant diversity in fishes. Although genetic variations in individual growth-regulated genes may impact the growth phenotype [18,19], the rapid genomic variation induced by hybridization and/or polyploidization is considered the most common and swift way of changing this phenotype in nature. Describing a phenomenon known as “heterosis”, if hybrid offspring exhibit faster growth rates and surpass the size of their parents, this trait is utilized to enhance agricultural production [20–23]. Researchers have extensively explored the genetic basis of heterosis, proposing three classic quantitative genetic hypotheses: dominance, overdominance, and epistasis. Moreover, some studies suggest that the emergence of heterosis may be linked to various molecular regulatory mechanisms, including genomic recombination [24], novel epigenetic modifications [25], and alterations in gene expression due to *trans*-regulatory factors from distinct species [26]. Additionally, research has indicated that the differential expression of alleles from different species is influenced by sequence differences in their regulatory regions [27]. In the case of orthologous genes from different genera, the greater sequence differences in their regulatory regions,

as compared to intraspecific and interspecific hybridization, will influence the reshaping of allele-specific expression (ASE) and its impact on the growth phenotype in their hybrid offspring. This aspect promises to be intriguing work.

To explore the impact of copy number variation (CNV) and mitochondrial regulation on ASE and growth traits, we collected 160 individuals representing six hybrid varieties derived from the intergeneric hybrid lineages of goldfish (2nRR) and common carp (2nCC). The integrated analyses of genomic, DNA methylation, and gene expression data provide a crucial foundation for our research. Our study will expand our understanding of gene interactions and their impact on phenotypes in animals.

## Results

### Determination of genotypes and growth phenotypes among hybrid varieties

Six hybrid varieties, comprising subgenomes R (originating from goldfish) and C (originating from common carp), were collected from individuals aged 8 months and 24 months after hatching, respectively (**Figure 1**A, Figure S1). To determine the ploidy levels of all hybrid individuals, flow cytometry was employed, using diploid goldfish (2n = 100) as the control group. To identify the source of mitochondrial genomes in reciprocal $F_1$ hybrids and allotriploid individuals with the same ploidy level, a fragment of the cytochrome b (*cytb*) gene in these hybrid individuals was obtained using Sanger sequencing. Subsequently, we compared the obtained sequences with those of goldfish and common carp to determine the origin of their mitochondrial genomes. Moreover, both whole-genome sequencing (WGS) and RNA sequencing (RNA-seq) data analyses were conducted to validate the genotypes of the six hybrid varieties. Based on the genomic data, the average depth of mapped reads of subgenomes R *vs.* C was approximately 1:1 in 2nCR, 1:2 in $3nRC_2$ and $3nC_2R$, and 2:1 in $3nCR_2$ and $3nR_2C$ (Tables S1–S3). Interestingly, we found that fish with identical subgenome ratios showed consistent distributions in the expression values of alleles R *vs.* C, as observed in the RNA-seq data (Figure 1B). Three clusters of gene expression profiles (cluster 1: 2nRC and 2nCR, cluster 2: $3nR_2C$ and $3nCR_2$, cluster 3: $3nC_2R$ and $3nRC_2$) remained stable across individuals (10–42 individuals in each variety) (Figure 1B). Similarly, analysis of the RNA-seq data clearly identified mitochondrial types (originating from goldfish or common carp) based on the different number of reads mapped to their two mitochondrial genomes, respectively (Tables S4 and S5). The above results can assist us in the initial identification of the genotype among the hybrid varieties and provide insights into their breeding strategies (Figure 1A).

Analyses of body length (BL), body height (BH), height of back muscle (HBM), and body

weight (BW) at 24 months after hatching showed that the growth rate was significantly higher in 2nCR compared to 2nRC (*t*-test; $P = 2.08 \times 10^{-24}$; two-tailed; $t = 2.02$; df = 42) (Figure 1C). Meanwhile, the allotriploid $3nC_2R$ and $3nRC_2$ (subgenomes R *vs.* C = 1:2) displayed faster growth rates compared to $3nCR_2$ and $3nR_2C$ (subgenomes R *vs.* C = 2:1) (*t*-test; $P = 4.13 \times 10^{-12}$; two-tailed; $t = 1.98$; df = 56) (Figure 1C). However, no significant difference in growth rate was observed between two fish with the same genotype ($3nCR_2$ and $3nR_2C$). Furthermore, a higher growth rate was detected in $3nRC_2$ (mitochondrial genomes originating from common carp) than in $3nC_2R$ (mitochondrial genomes originating from goldfish) (*t*-test; $P = 0.0001$; two-tailed; $t = 2.01$; df = 46) (Figure 1C), while there is the same nuclear genome in them (Figure 1A). These findings indicate that more sets of subgenome C and mitochondrial genomes originating from 2nCC contribute to the large body size or rapid growth rate among these hybrid varieties.

**High CNVs in subgenome R**

Previous studies demonstrated that gene conversion occurred in the assembled genome of allotetraploid fish [15]. The diverse CNVs between somatic and germ cells were found in the interspecific $F_1$ and allotetraploid populations, revealing various mitotic and meiotic CNVs associated with gene conversion [5,15]. To investigate the presence of different CNVs in allotriploid progenies, obtained from the backcrossing of allotetraploid to diploid goldfish or common carp, we conducted WGS on seven individuals of the $F_1$ hybrid and 22 individuals of triploids (8 months after hatching) (Tables S1 and S2). CNV detection for 1545–3017 genes in the 2nRC and triploid varieties revealed a higher CNV ratio in subgenome R (49.25%–83.33%) than in subgenome C (16.67%–50.75%) (*t*-test; $P = 4.02 \times 10^{-21}$; two-tailed; $t = 2.00$; df = 56), indicating a leading role of subgenome R in the genome plasticity of hybrid varieties (**Figure 2**A; Table S6). Focusing on 46,424 species-specific genes (SSGs) (24,283 in 2nCC and 22,141 in 2nRR) and 18,020 allelic gene pairs (AGPs), the majority of genes with CNVs (71.55%–85.55%) belonged to SSGs and exhibited a higher ratio of genome variation in SSGs than in AGPs (*t*-test; $P = 1.80 \times 10^{-53}$; two-tailed; $t = 2.00$; df = 56) (Tables S6 and S7).

We investigated the distribution of CNVs in allelic genes. We observed a higher frequency of copy number increase events in allele R (52.65%–74.43%) than in allele C (25.57%–47.35%) (*t*-test; $P = 1.04 \times 10^{-43}$; two-tailed; $t = 2.05$; df = 28) (Table S7). In some individuals, CNV events occurred on long chromosomal segments involving contiguous genes or entire chromosomes (Figure S2). For example, CNV events occurred on the entire chromosome 40 (chr40) in the $3nR_2C$-4 individual. In the $3nRC_2$-2 individual, CNV events occurred on the parts of chr19 (92 genes) and chr36 (63 genes), as well as the entire chr25 and chr31. These CNV events resulted in a 1:1 ratio of gene copy numbers

from the inbred parents in these allotriploid individuals (Figure 2B, Figure S2).

Furthermore, WGS data revealed allele loss caused by CNVs. Among the 22 allotriploid individuals, the number of allele loss events ranged from 2 to 223, while none were observed in the $F_1$ hybrids (Table S7). For instance, the loss of allele C in contiguous genes on chr19 was observed in two individuals of $3nR_2C$ and one individual of $3nCR_2$ (Figure 2B, Figure S2). We speculated that the shared allele loss observed in different triploid progenies may be derived from the gametes of the same paternal $4nR_2C_2$ individual through interploid hybridization. Interestingly, the loss of allele C was detected in the 92 contiguous genes of $3nCR_2$-4, which also exhibited the highest growth rate among the $3nCR_2$ population. Gene Ontology (GO) analysis of these 92 genes identified *rfx3* and *gpat4* as being annotated to epithelial cell maturation (GO: 0002071, *P* value = 0.001). We speculate that the loss of allele C in these two genes may contribute to the high growth rate observed in the allotriploid.

**CNVs altering ASE**

To investigate the impact of CNVs on allelic expression, we conducted integrated genomic and expression analyses using muscle tissue samples from 7 individuals of the $F_1$ hybrid and 22 individuals of the allotriploids (Table S2). Specifically, we focused on the loss of allele C in $3nR_2C$ and $3nCR_2$, comparing the gene expression values between no-CNV (no allelic loss) and those with CNV (allelic loss) within the corresponding population. In the $3nRC_2$-2 individual, where CNVs led to a 1:1 allelic copy number ratio (Figure 2B), genes within the CNV region also displayed a 1:1 allelic expression ratio (Figure 2C). Conversely, genes outside the CNV regions exhibited a 1:2 allelic expression ratio (Figure 2C). Then, differential expression analysis was performed between CNV and no-CNV individuals in the $3nRC_2$ population, and significant differences were detected in chr19, chr25, chr31, and chr36 (Figure 2D). These findings suggest that copy number changes in the hybrids could affect gene expression, highlighting the effects of CNVs on allelic expression.

**Mitochondrial regulation shaping ASE and species-specific expression**

Distinct mitochondrial genomes and the same nuclear genome were in two groups (diploid group 1: 2nRC and 2nCR, triploid group 2: $3nRC_2$ and $3nC_2R$). This provided valuable insights into mitochondrial genetics and its role in regulating growth diversity through gene expression (Tables S1, S2, and S8). Comparative analyses revealed that 6516 genes (7.9%) of the total 82,464 genes (alleles R and C considered independent genes) differed in expression between the reciprocal $F_1$ hybrids (13 individuals in 2nRC and 2nCR), while only 126 genes (0.15%) showed differential expression between $3nRC_2$ and $3nC_2R$ (10 individuals). The lower number of differentially expressed genes

184 (DEGs) in triploids compared to diploids may be caused by the high frequency of CNVs disrupting
185 ASE regulated by mitochondrial genetics (**Figure 3**A).
186 In the diploid group, the analysis of differential gene expression revealed that in subgenome R,
187 AGPs (1834) had more DEGs compared to SSGs (1440), whereas in subgenome C, SSGs (1734) had
188 more DEGs than AGPs (1508) (Pearson's chi-squared test; $P = 2.04\times10^{-14}$; $\chi^2 = 58.497$; df = 1)
189 (Table S9). This suggests that orthologous genes from goldfish and SSGs from common carp are
190 more susceptible to regulation by maternal effects, resulting in differential expression between
191 reciprocal $F_1$ hybrids. Furthermore, we detected that highly expressed genes in 2nRC were
192 predominantly in allele R (1881) rather than in allele C (1545), while the opposite trend was
193 observed in 2nCR, where highly expressed genes were more in allele C (1697) than in allele R (1393)
194 (Figure 3A). This finding suggests that mitochondria in hybrids may preferentially upregulate the
195 expression of nuclear genes from the same species. Interestingly, we noticed that allele R in *ptf1a*
196 was silenced in 2nCR, whereas its expression was detected in 2nRC, indicating that the
197 mitochondrial genes originating from 2nCC inhibited the expression of allele R (Figure 3A). The
198 significant diversity in allelic gene expression between 2nRC and 2nCR, resulting from the silencing
199 of allele R in *ptf1a*, may be linked to their distinct growth rates [28].
200 To further investigate the magnitude of independence and interaction between alleles R and C,
201 we established nine expression patterns for alleles R and C (Figure 3B). Out of these, 2754 genes
202 (15.28%) in the diploid group (2nRC and 2nCR) and 52 genes (0.28%) in the triploid group
203 exhibited expression changes regulated by distinct mitochondrial genetics. In the diploid group, we
204 found that the expression of either allele R or C was altered in specific patterns (II, IV, VI, and VIII)
205 across 2167 genes (12.02%). These patterns indicate the existence of independent regulatory
206 networks connecting mitochondrial genes to the expression of alleles R or C (Figure 3B; Figure S3).
207 Additionally, a shared regulatory network in mitochondrial genetics regulating both alleles R and C
208 (patterns III and IX) was observed in 572 genes (3.17%) (Figure 3B, Figure S3). Interestingly, we
209 observed an opposite trend between the expression of alleles R and C in 15 genes (0.08%, patterns I
210 and VII), which was likely related to an antagonistic relationship between the regulatory networks of
211 the distinct alleles. These results showed the diversified regulatory networks in mitochondrial
212 genetics that regulate allelic gene expression.
213
214 **Gene coexpression analyses revealing genetic networks underlying growth rate diversity**
215 The above results demonstrated that the diversified ASE and species-specific expression were in the
216 six hybrid varieties. We then used a weighted gene correlation network analysis to detect gene
217 coexpression networks and genetic modules in the 131 individuals (24 months after hatching).

Twelve modules were identified based on the correlation of the expression profiles of the 65,495 expressed genes (31,974 genes in subgenome R, 33,521 genes in subgenome C) (Figure S4A). Among these modules, Module Eigengene 1 (ME01) exhibited the highest correlation with growth-related phenotypic values, including BW and BL, while a significant correlation was detected between gene significance and module membership ($r$ = 0.81, $P = 1 \times 10^{-20}$) (Figure S4B). After gene filtering, we identified 3693 genes within ME01 as candidate growth-regulated genes. Within this module, the coexpression network reveals that the 3672 genes in subgenome R and the 21 genes in subgenome C showed significant correlations between gene expression and BW (**Figure 4**A). These results indicate that CNVs in subgenome R, along with changes in gene expression within subgenome R, are primarily responsible for regulating growth diversity in these hybrid varieties.

To further identify the relationship between the expression of the 3693 growth-regulated genes and BW, we analyzed gene expression diversity and BW diversity across individuals. The highest diversities of gene expression and BW were observed in $3nR_2C$, while the lowest diversities were observed in $3nC_2R$ (Figure 4B). Importantly, both $3nR_2C$ and $3nCR_2$ (with two sets of subgenome R) exhibited higher diversities in gene expression and BW compared to $3nRC_2$ and $3nC_2R$ (with one set of subgenome R). These findings, coupled with the enrichment of CNVs in subgenome R, indicate that the high CNV ratio in subgenome R contributes to the increased diversity of allele R expression, which subsequently leads to the diversification of growth phenotypes in the hybrid population (Figure 2, Table S6). In the diploid group, higher gene expression diversity was detected in 2nRC than in 2nCR (Figure 4B), suggesting that the maternal effects related to goldfish-originated regulation may be more beneficial to the CNV of allele R and result in gene expression diversity across individuals.

Among the 3693 growth-regulated genes, we found that the expression of 3672 genes in subgenome R and one gene (*slc2a12*) in subgenome C exhibited negative correlations with BW, while the other 20 genes in subgenome C showed positive correlations (Figure 4A). Additionally, the expression of these 20 genes was found to be higher in the 2nCR, $3nRC_2$, and $3nC_2R$ populations compared to the 2nRC, $3nR_2C$, and $3nCR_2$ populations (Figure 4C). We compared gene expression data from 24-month-old individuals (n = 132) with data from 8-month-old individuals (n = 29). Genes exhibiting strong positive correlations [Pearson correlation coefficient (PCC) > 0.5] between BW and gene expression in the larger dataset also showed strong positive correlations in the smaller dataset, with the exception of the *prvb* gene (PCC = 0.37, $P$ value = 0.05) (Figure S5). Interestingly, the expression of *slc2a12* in subgenome C exhibited a positive correlation with BW at low water temperature (about 8℃, 8 months after hatching) (PCC = 0.67, $P$ value = 0.003) (Figure S5), while a

negative correlation was detected at high water temperature (about 20℃, 24 months after hatching) (Figure 4A and C). The opposite correlations were likely related to the different strategies for rapid growth rate of these hybrid individuals in alternation with the seasons, in which the up-regulated expression of *slc2a12* in subgenome C could decrease the amount of exercise and energy consumption at low temperatures (winter), while the down-regulated expression could increase the amount of exercise for obtaining food at high temperatures (spring) [29].

**Variations in gene regulatory networks and their effects on growth rate**

The decreased expression of genes in subgenome R and the increased expression of genes in subgenome C both contributed to the rapid growth rate, prompting the question of how variations in gene regulatory networks regulated allelic expression and growth diversity. Among the 3693 growth-regulated genes, 2094 were orthologous genes, while 1587 were SSGs in subgenome R and 12 were SSGs in subgenome C (Figure S6). The PCC values of the 3693 growth-regulated genes were higher in the 2094 AGPs than in non-AGPs (ANOVA $F$-test = 0.85, df = 2081, $P$ = 0.000123) (**Figure 5**A). This finding suggests that shared *trans*-regulatory factors between alleles R and C homogenize the expression levels of the two orthologous genes originating from goldfish and common carp, leading to increased synchrony in the allelic expression in hybrids. In the analysis of PCC between 2094 AGPs, 832 (39.73%) displayed a positive correlation (PCC > 0.3), with 304 (14.52%) exhibiting a strong positive correlation (PCC > 0.5). In contrast, only 12 AGPs (0.57%) displayed a negative correlation (PCC < −0.3), and no AGPs exhibited a strongly negative correlation (PCC < −0.5). These results reflect a synchrony of allelic expression in 40.30% of genes and independence in 59.70% of genes. Furthermore, we analyzed nine AGPs where the expression of allele C exhibited a strong positive correlation (PCC > 0.5) with BW (Figure 5B). Among these nine AGPs, six also showed a strong positive correlation (PCC > 0.5) between the expression values of alleles R and C (Figure 5B). Interestingly, higher PCC values of two alleles and lower BWs were observed in 2nRC than in 2nCR, and the same phenomenon was detected in $3nR_2C$ and $3nCR_2$ than in $3nRC_2$ and $3nC_2R$ (Figure 5C). Among hybrids with the same ploidy level, more diversified gene regulatory networks between alleles of growth-regulating genes may be associated with faster growth. This result sheds light on why heterosis often appears in hybrid $F_1$ generations, and with successive generations of hybrid offspring, the heterosis diminishes or decreases [20–24]. This phenomenon might be attributed to the presence of complete *trans*-regulatory factors from different species only in hybrid $F_1$, leading to the maximization of differences in the gene regulatory network between allelic genes.

The PCC values between alleles could also allow us to assess the variation of gene regulatory networks among the six hybrid varieties. The highest difference was observed between $3nR_2C$ and $3nRC_2$ (*t*-test; $P = 6.9 \times 10^{-152}$; two-tailed; $t = 1.96$; df = 2084) (Figure 5D), which had distinct mitochondrial genomes and different subgenome ratios of R *vs.* C (Figure 1A). We further investigate the differences in gene regulatory networks influenced by mitochondrial genetics in the two reciprocal $F_1$ hybrids (*t*-test; $P = 2.66 \times 10^{-6}$; two-tailed; $t = 1.96$; df = 2084) (Figure 5D). Reversed PCC values were observed in 310 growth-regulated AGPs (Table S10). Further analysis of the strong positive correlation (PCC > 0.5) between the expression of two alleles revealed that only 194 AGPs (10.35% of 1874 AGPs) were shared among the six hybrid varieties, while 438 common AGPs were observed between the two $F_1$ hybrids and 362 common AGPs were identified among the four triploid varieties (Figure 5E, Figure S7). Further, 2nCR and $3nRC_2$ exhibited similar PCC in allelic gene expression (*t*-test: $P = 0.80$; two-tailed; $t = 1.96$; df = 2084), raising the question of why these hybrids with different ploidy levels exhibited similar gene regulatory networks. Recent studies revealed that DNA methylation inhibits the transcription of genes in the additional subgenome C of $3nRC_2$ (**Figure 6**A) [30], which may account for the similar gene regulatory networks between 2nCR and $3nRC_2$. The above results revealed a high divergence of gene regulatory networks between alleles in these hybrid varieties.

**Allele-specific DNA methylation regulating growth rate diversity**

Through analyses of DNA methylation in the 3693 growth-regulated genes, we tried to investigate whether and how DNA methylation affects growth rates through regulating ASE. So we analyzed whole-genome bisulfite sequencing data (the muscles of 2nRR, 2nCC, $3nR_2C$, and $3nRC_2$) and growth phenotype data (a significant difference in BW between $3nR_2C$ and $3nRC_2$) to investigate the contribution of DNA methylation to subgenomes R and C [30]. After mapping clean reads to the combined genome of 2nRR and 2nCC, the uniquely mapped reads were used to assess the methylation levels in CpG islands. Comparative analysis revealed that the DNA methylation level in each subgenome was higher in the two triploids ($3nR_2C$ and $3nRC_2$) than in their inbred parents (2nRR and 2nCC) (Figure 6A), indicating that high DNA methylation suppressed gene expression in triploids.

We focused on 2094 genes that are involved in growth regulation, and we compared the DNA methylation levels of the alleles R and C in $3nR_2C$ and $3nRC_2$. We found that allele R showed lower DNA methylation in $3nR_2C$ than in $3nRC_2$, while its expression was higher in $3nR_2C$ (Figure 6B and C). On the other hand, allele C showed higher DNA methylation in $3nR_2C$ and lower expression compared to $3nRC_2$ (Figure 6B and C). Comparing $3nR_2C$ and $3nRC_2$, we identified 84 differentially

methylated genes (DMGs) (4.06%) from AGPs and 57 DMGs (3.56%) from SSGs (Table S11). The majority of DMGs (AGP: 73 of 84, SSG: 46 of 57) had reduced DNA methylation in $3nR_2C$ (Table S11), indicating that the lower DNA methylation in subgenome R contributed to the higher expression levels of allele R in $3nR_2C$ compared to $3nRC_2$. Indeed, histological examination of skeletal muscle tissues using hematoxylin and eosins (H&E) staining uncovered that the cross-sectional area of myofibers was bigger in 2nCC than in 2nRR, which was likely related to the difference in skeletal muscle development between the two species (*t*-test; $P = 3.18 \times 10^{-16}$; two-tailed; $t = 2.00$; df = 56) (Figure 6D). We detected a larger cross-sectional area of myofibers in $3nC_2R$ than in $3nR_2C$, suggesting that the high expression of allele C benefited the growth of myofibers (*t*-test; $P = 1.40 \times 10^{-5}$; two-tailed; $t = 2.00$; df = 56) (Figure 6D). In conclusion, our findings indicate that the regulation of DNA methylation may contribute to the differential activity of ASE and growth rates between $3nC_2R$ and $3nR_2C$, possibly explaining the variations in their growth rates.

## Discussion

Using different hybrid strategies that produce the controlled genotypes of hybrids, we characterized the mitochondrial and nuclear genetic variants associated with variations in gene expression and growth diversity. We detected the CNVs of subgenomes R and C across hybrid individuals, including allele loss in triploids, and found their effects on allele-specific and species-specific expressions. Applying a weighted gene correlation network analysis, we identified 3693 genes as candidate growth-regulated genes, in which the expression of 2094 AGPs and 1599 SSGs exhibited a significant correlation with growth diversity. Using correlation analyses between the expression of distinct alleles R and C, we detected the different degrees of independence and interactions in the allelic regulatory networks, which reflected variations of gene regulatory networks among different hybrid varieties. Importantly, we found that the diversified gene regulatory networks of distinct alleles R and C in growth-regulated genes may contribute to the rapid growth rate. This result suggests that maintaining and increasing differentiation in allelic expression will result in the emergence of heterosis and be beneficial for aquaculture and animal breeding. In addition, we revealed that DNA methylation shaped allelic expression variations in subgenomes R and C.

Following their divergence 10 Mya, high genome plasticity in goldfish and common carp facilitated diverse growth phenotypes during domestication [8,31,32]. Now, we detected diverse CNVs in the nascent allotetraploid population ($4nR_2C_2$, $F_3$–$F_{28}$) [15,33], which were derived from the hybridization of goldfish and common carp [5,14], and provided abundant genetic diversities in their

351 allotriploid progenies through different interploid crossings with their inbred parents [16].
352 Meanwhile, the random emergence of repair DNA damage during mitosis also resulted in CNVs,
353 including allele loss in triploid individuals. Joint analyses of the CNV region, growth rate, and
354 functional annotation data could provide an effective way to identify causal genes associated with the
355 growth variation in inter- and intra-hybrid populations. For example, we showed that the loss of
356 allele C in *rfx3* and *gpat4* might have contributed to the high growth rate. The majority of CNVs in
357 the hybrid varieties were distributed in subgenome R, where dynamic transposition of transposable
358 elements could result in CNVs and allelic expression variation and increase growth diversity [15].

359 Diverse subgenome ratios, mitochondrial genetics, and CNVs provide abundant genetic materials
360 for investigating the relative contribution of gene regulatory networks to the variations in
361 allele-specific and species-specific expressions. When exposed to the common *trans*-acting
362 regulatory factors, the distinct *cis*-regulatory elements in allelic genes may cause a target gene to
363 interact or bind differentially with the transcriptional factors, thus resulting in differential expression
364 between alleles [34,35]. We showed that the dominance of *trans*-acting regulatory effects decreased
365 the expression diversity of alleles in most genes, while *cis*-regulatory regulatory effects increased it
366 in a few genes [36,37]. Different *trans*-acting influences involving mitochondrial regulation in the
367 reciprocal $F_1$ hybrids reflect differential expression of SSGs primarily in subgenome C, which play
368 key roles in growth diversity. Additionally, the distinct subgenome ratios in allotriploids also shape
369 allelic CNVs and alter the dosage of the *trans*-acting factors between alleles, although the diverse
370 effects of DNA methylation occur in different subgenomes [26,38]. Our findings indicate that
371 dynamic changes in variations of gene regulatory networks increase the magnitude of independence
372 and interactions in allelic regulatory networks, resulting in a great increase in allelic expression
373 variation and growth diversity in these intergeneric hybrid varieties.

374 A previous study indicated that the expression dominance in allele R was beneficial to high BH
375 in allotriploids, while the expression dominance in allele C was beneficial to high BL [30]. We
376 showed that the decreased expression of genes in subgenome R and the increased expression of
377 genes in subgenome C contributed to the rapid growth rate. These findings suggest that the
378 appropriate combination of ASE may contribute to the heterosis in quantitative traits. Interestingly,
379 *slc2a12* belongs to a family of transporters that catalyze the uptake of sugars through facilitated
380 diffusion [39]. The increased expression of *slc2a12* in winter could decrease the amount of exercise
381 and energy consumption in low temperatures, while the decreased expression of *slc2a12* in spring
382 could increase the amount of exercise needed to obtain food [29]. These different strategies in
383 alternation with the seasons will increase the growth rates of these hybrid individuals. Our result
384 provided new viewpoints: the great diversity in *cis*-regulatory sequences between distinct alleles

could decrease the synergy of ASE and increase the magnitude of heterosis in the growth rate. In summary, our findings shed light on how the regulatory network underlying distinct subgenomes regulates growth plasticity.

## Conclusion

The allotriploid obtained through interploidy hybridization between allotetraploid and diploid has the advantages of ecological friendliness (sterility) and a fast growth rate, which have made contributions to fish breeding for more than 20 years in China. It has been a huge challenge for us to figure out how to improve the allotriploid fish even more. Our results revealed that variations in CNVs and gene regulatory networks between alleles could shape the growth diversity in the hybrid populations. Consequently, selecting individuals with low-copy growth-regulated genes from allele R (originating from goldfish) and high-copy growth-regulating genes from allele C (originating from common carp) will contribute to the breeding of allotriploid populations exhibiting a rapid growth phenotype. These studies will help us develop a novel hybrid breeding strategy through the genotype selection of parental allotetraploids.

## Materials and methods

### Collection and determination of samples

The fish used in this study included an $F_1$ diploid hybrid (2nRC) obtained from hybridization between *C. auratus* red var. (goldfish, 2nRR, ♀) and *C. carpio* (common carp, 2nCC, ♂), an $F_1$ diploid hybrid (2nCR) obtained from hybridization between 2nCC (♀) and 2nRR (♂), an allotriploid ($3nR_2C$) obtained from interploid crossing of 2nRR (♀) with a allotetraploid of 2nRR × 2nCC ($4nR_2C_2$, ♂), a allotriploid ($3nRC_2$) obtained from interploid crossing of 2nCC (♀) with $4nR_2C_2$ (♂), a allotriploid ($3nCR_2$) obtained from interploid crossing of an allotetraploid of $4nR_2C_2$ (♀) with 2nRR (♂), a allotriploid ($3nC_2R$) obtained from interploid crossing of $4nR_2C_2$ (♀) with 2nCC (♂). These hybrid varieties, including two reciprocal $F_1$ hybrids (2nRC and 2nCR) and four triploids ($3nR_2C$, $3nRC_2$, $3nCR_2$, and $3nC_2R$), were fed in separate pools under identical environmental conditions. These conditions included suitable water temperatures, oxygen levels, food supply, breeding density, *etc*. These pools were located in the drainage area of Dongting Lake, Hunan, China (29°11'51" N, 112°35'50" E). Some growth traits, including BL, BH, HBM, and BW, were detected in multiple growth stages. Twenty-nine healthy individuals (eight months after hatching, 7 in 2nRC,

4 in $3nR_2C$, 7 in $3nRC_2$, 8 in $3nCR_2$, and 3 in $3nC_2R$) and 131 healthy individuals (24 months after hatching) were collected for this study, respectively. These hybrid varieties were deeply anesthetized with 300 mg/l tricaine methanesulfonate (MS-222, Sigma-Aldrich, St. Louis, MO) for 10 min (25°C) in a separation tank. After confirming the death, all samples were collected for dissection. The DNA content of erythrocytes from 2nRR, 2nCC, and the hybrids was measured using flow cytometry (Cell Counter Analyzer, Partec GmbH, Otto-Hahn-Strasse 32, D-48161 Munster, Germany) for identifying chromosome number [40].

**DNA isolation and genomic sequencing**

High-quality genomic DNA of 2nRR, 2nCC, and the hybrids was isolated from the muscle tissue using DNeasy Blood & Tissue Kits (QIAGEN, no. 69504, Hilden, Germany). The quality of DNA was checked by a NanoDrop® ND-1000 Spectrophotometer (Thermo Fisher Scientific, Inc., Wilmington, DE) with 260/280 and 260/230 ratios. The type of mitochondrial genome in the hybrids was identified based on a fragment of *cytb*. Then, the high-quality DNA was used to construct a paired-end library (150 bp × 2) and sequenced by Illumina HiSeq X Ten Sequencing System (Illumina, San Diego, CA) according to standard protocol. The detail was as follows: a mixture containing equal amounts of 2nRR and 2nCC DNA, the muscle of 29 hybrid individuals. After obtaining the raw data, the sequencing adaptors were removed. fastp (v. 0.21.0) was used to remove duplicate read pairs and low-quality reads based on the default parameters [41].

**Detection of CNV**

High-quality reads in the hybrid were mapped to the combined nuclear and mitochondrial genomes of goldfish [8] [nuclear DNA (nDNA): PRJCA001234 of National Genomics Data Center (NGDC) database, mitochondrial DNA (mtDNA): AY714387.1] and common carp [32] [nDNA of Yellow River carp: PRJNA510861 of National Center of Biotechnology Information (NCBI) database, mtDNA: AP009047.1] using BWA with the default parameters. Coordinate-sorted BAM output files of WGS were obtained to calculate the number of mapped reads in the coding region of each gene using htseq-count (v. 0.12.4) with thresholds of "-m union --nonunique = none". The gene per million (GPM) is a value to measure how many reads are mapped to each gene in genomic data. It helps us understand the relative abundance of gene copies in a sample by considering the length of the gene and the total number of reads. The formula for calculating GPM is as follows:

$$\mathrm{GPM} = \mathrm{A} \times \frac{1}{\sum \mathrm{A}} \times 10^6, \text{ where } \mathrm{A} = \frac{\text{total reads mapped to gene} \times 10^6}{\text{gene length (bp)}}$$

For *in silico* $F_1$, we sequenced an equal mixture of 2nRR and 2nCC DNA using the same

449 sequencing platform as other genomic data. By comparing the hybrid varieties with the *in silico* $F_1$,
450 we were able to detect CNVs in all the hybrid varieties. To identify CNVs, we set thresholds based
451 on the genotype. We used the logarithm base 2 of the ratio ($GPM_{hybrid}/GPM_{mixed}$) and compared it to
452 $\log_2(\frac{B\times2}{C})$ and $\log_2(\frac{B\times0.5}{C})$. If the logarithm base 2 of ($GPM_{hybrid}/GPM_{mixed}$) was greater than $\log_2(\frac{B\times2}{C})$
453 or less than $\log_2(\frac{B\times0.5}{C})$, it was considered a CNV. In this formula, "B" represents the allelic ratio (R
454 or C) in hybrids, and "C" represents the allelic ratio (R or C) in *in silico* $F_1$. for 2nRC, "B" is $\frac{1}{2}$; for
455 allele R of $3nRC_2$ and $3nC_2R$, and allele C of $3nR_2C$ and $3nCR_2$, "B" is $\frac{1}{3}$; for allele C of $3nRC_2$ and
456 $3nC_2R$, and allele R of $3nR_2C$ and $3nCR_2$, "B" is $\frac{2}{3}$.

457 AGPs between the subgenomes R (originating from 2nRR) and C (originating from 2nCC) in the
458 hybrid varieties, including the $F_1$ hybrids (2nRC and 2nCR) and four triploids ($3nR_2C$, $3nRC_2$,
459 $3nCR_2$, and $3nC_2R$), were obtained using the all-against-all reciprocal BLASTP (v. 2.8.1) with an
460 e-value of $1E^{-6}$ based on protein sequences. Then, transcripts that lacked gene annotation and were
461 shorter than 300 bp were discarded from AGPs. GPM values in each AGP could be used to assess
462 allelic CNVs between the subgenomes R and C in the hybrid varieties. The values of $\log_{10}((R_{GPM\ in}$
463 $_{hybrid}/C_{GPM\ in\ hybrid}) - (R_{GPM\ in\ mixed}/C_{GPM\ in\ mixed}))$ could be used to assess the allelic CNVs. The detail
464 thresholds for them were set up based on the genotype as follows: (1) $\log_{10}(2)$ and $\log_{10}(0.5)$ in $F_1$
465 hybrid (2nRC and 2nCR); (2) $\log_{10}(4)$ and $\log_{10}(1)$ in $3nR_2C$ and $3nCR_2$;( 3) $\log_{10}(1)$ and $\log_{10}(0.25)$
466 in $3nC_2R$ and $3nRC_2$.

467

468 **RNA isolation and RNA-seq**

469 To obtain gene expression profiling of the two reciprocal $F_1$ hybrids and allotriploids, total RNA of
470 the muscle tissue was isolated and purified according to a TRIzol extraction method [42]. The RNA
471 concentration was measured using NanoDrop technology (NanoDrop ND-1000 UV/Vis
472 spectrophotometer, NanoDrop Technologies Inc., Wilmington, DE, US). Total RNA samples were
473 treated with DNase I (Cat. No. 18068-015; Invitrogen, Thermo Fisher Scientific, Inc., Philadelphia,
474 PA, USA) to remove any contaminating genomic DNA. The purified RNA was quantified using a
475 2100 Bioanalyzer system (Agilent, Santa Clara, CA, USA cat #5067-5576). Isolated messenger RNA
476 (mRNA) was fragmented with a fragmentation buffer. The resulting short fragments were reversely
477 transcribed and amplified to produce complementary DNA (cDNA). Illumina RNA-seq libraries of
478 the 29 samples were prepared according to the standard high-throughput method. The quality of the
479 cDNA library was assessed by the 2100 Bioanalyzer system (Agilent, Santa Clara, CA, USA cat
480 #5067-5576). The library was sequenced with a paired-end (2 × 150 bp) setting using the Illumina

HiSeq X Ten Sequencing System (Illumina, San Diego, CA). The transcriptome data of muscle tissue in 131 hybrid individuals was obtained using DNA nanoball technology using DNBSEQ-T7 (MGI, Shenzhen, China) according to the standard method [43]. Then, low-quality bases and adapters were trimmed out using fastp (v. 0.21.0). The high-quality reads were used in the next analyses.

**Detection of gene expression based on RNA-seq**

All RNA-seq reads of 2nRR, 2nCC, and the hybrids were mapped to the combined nuclear and mitochondrial genomes of *C. auratus* red var. [8] and *C. carpio* [32] using HISAT2 [44] (v. 2.1.0) with default parameters. Then, the mapped files were handled with SAMtools (v. 1.10) [45], while the unique mapped reads were obtained using htseq-count (v. 0.12.4) [46]. The expression value was normalized based on the ratio of the number of mapped reads for each gene to the total number of mapped reads for the entire genome. The transcripts per million (TPM) values were calculated based on the normalized data. These reads in the $F_1$ hybrid and four triploids were used to calculate the expression values of the genes in subgenomes R and C [47]. The genes with mapped reads in each sample < 10 and TPM values < 1 were not used in our next analyses. Differential expression analysis was performed using DESeq2 of the R package with the below thresholds: fold change > 3, *P* value < 0.001, and *P* adjusted < 0.001. Differential expression analysis was performed in 13 individuals of the diploid group (2nRC and 2nCR) and in 10 individuals of the allotriploid group ($3nRC_2$ and $3nC_2R$).

Both WGS and RNA-seq were performed in the 29 individuals (eight months after hatching, 7 in 2nRC, 4 in $3nR_2C$, 7 in $3nRC_2$, 8 in $3nCR_2$, and 3 in $3nC_2R$) for investigating the effects of CNVs on ASE and species-specific expression, which were assessed based on the above thresholds of differential expression analysis.

**Weighted gene correlation network analysis and functional annotation**

To investigate expression patterns across samples, we conducted coexpression analysis based on the two $F_1$ hybrid and triploid samples using weighted gene correlation network analysis (v. 1.67). An unsupervised network on gene expression was built using the following default parameters. First, a matrix of Pearson correlations between genes was generated based on expression values. Then, an adjacency matrix representing the connection strength among genes was established by raising the correlation matrix to a soft threshold power. Next, the adjacency matrix was used to calculate a topological overlap matrix. Genes with similar coexpression patterns were clustered using hierarchical clustering of dissimilarity. Pearson correlations between the expression level of that gene and module were performed using eigengene-based connectivity, while Pearson correlations were

further calculated to measure the strength and direction of association between modules and growth traits. The coexpressed modules were determined and used in our next functional analyses. The hub genes related to growth regulation were further filtered based on thresholds of module membership > 0.8 and gene significance > 0.3. Functional enrichment analyses were conducted and annotated with GO and Kyoto Encyclopedia of Genes and Genomes (KEGG) databases. The standard deviation of BW divided by the average BW across individuals was used to assess the BW diversity in each population. The standard deviation of the TPM value across the individuals of the six hybrid varieties was used to assess the expression diversity of the predicted growth-regulated genes.

**Correlation in the expression of alleles R and C, correlation between growth traits and allelic expression**

We detected a PCC between the expression of alleles R and C based on the below thresholds: a positive correlation was settled as PCC > 0.3; a strongly positive correlation was settled as PCC > 0.5; a negative correlation was settled as PCC < −0.3; a strongly negative correlation was settled as PCC < −0.5. Differential analysis was performed based on the *P* value using a *t*-test. Then, we performed Pearson's correlation analysis between growth weight and the expression of allele R or C.

**Mapping of methylation sequencing data and differentially methylated analysis**

The whole-genome bisulfite sequencing data of 2nRR, 2nCC, $3nR_2C$, and $3nRC_2$ (muscle tissue, 2 years old, three biological replicates in each variety) were obtained from NGDC database with BioProject accession: PRJCA003625. After quality checking of the methylation sequencing reads, the clean reads of 2nRR and 2nCC were mapped to the respective genomes, and the clean reads of the two triploids ($3nR_2C$ and $3nRC_2$) were mapped to the combined genome sequences of 2nRR and 2nCC [8,32]. The Bismark analysis pipeline was used to detect the methylated loci with the mapped parameters (-score_min L, 0, −0.2 −X 1000 -no-mixed -no-discordant) [48,49]. The clean reads were used for mapping to the reference genome four times, and only the reads that mapped to the same position of the reference genome each time were retained in our next analysis. A binomial distribution test was performed to identify 5-methylcytosine for each cytosine site. The potential methylation sites were then checked using the depth > 4 and false discovery rate (FDR) < 0.05 thresholds.

The average CpG methylation was detected in different gene regions, including upstream (a window size of 100 bp for 2 kb regions), the gene body, and downstream (a window size of 100 bp for 2 kb regions) of the coding regions. The average CpG methylation in the upstream and downstream transposon regions (2 kb) was calculated and plotted using R. The regions with different

549 methylation were detected using MOdel based Analysis of Bisulfite Sequencing data (MOABS) [50].
550 The R packages Dispersion Shrinkage for Sequencing data (DSS) and bsseq were used to call
551 differentially methylated regions and predict DMGs based on a *P* value < 0.01.
552
553 **H&E staining**
554 A 10 mm trunk muscle from 2nRR, 2nCC, $3nR_2C$, and $3nRC_2$ was dissected from the region in the
555 dorsum and fixed in Bouin's solution for 24 h. The fixed tissues were washed with distilled water for
556 4 h at 20℃. After dehydration in ethanol gradients and xylene, the samples were fixed in 4%
557 paraformaldehyde and cut into serial paraffin sections (5–7 μm in thickness). Sections were
558 processed for H&E staining. Digital images were captured with a microscope (DX8, Olympus,
559 Tokyo, Japan). Three independent biological replicates were used to collect quantitative data on
560 H&E staining in each hybrid variety.
561

562 ## Ethical statement

563 All procedures performed on animals were approved by the Academic Committee at Hunan Normal
564 University, Hunan, China (Approval No. 2018D013).
565

566 ## Data availability

567 The raw reads of WGS and RNA-seq data have been deposited in the Genome Sequence Archive [51]
568 at the NGDC, Beijing Institute of Genomics (BIG), Chinese Academy of Sciences (CAS) / China
569 National Center for Bioinformation (CNCB) (GSA: CRA009160 for WGS data for 29 individuals,
570 CRA009161 for RNA-seq data for 29 individuals, and CRA009164 for RNA-seq data for 131
571 individuals; BioProject: PRJCA013677), and are publicly accessible at https://ngdc.cncb.ac.cn/gsa) .
572 The raw reads of equally mixed DNA from goldfish and common carp have been deposited in
573 BioSample at the NGDC, BIG, CAS / CNCB (BioSample: SAMC449140), and are publicly
574 accessible at https://ngdc.cncb.ac.cn/gsa/browse/CRA003321/CRX269785.
575

576 ## CRediT author statement

577 **Li Ren:** Conceptualization, Data curation, Formal analysis, Writing – original draft, Project
578 administration, Writing – review & editing, Validation, Funding acquisition. **Mengxue Luo:** Data
579 curation, Writing – review & editing, Validation. **Jialin Cui:** Investigation. **Xin Gao:** Data curation,
580 Investigation. **Hong Zhang:** Investigation. **Ping Wu:** Investigation. **Zehong Wei:** Investigation.
581 **Yakui Tai:** Investigation. **Mengdan Li:** Investigation. **Kaikun Luo:** Investigation. **Shaojun Liu:**

Conceptualization, Project administration, Validation, Funding acquisition. All authors have read and approved the final manuscript.

## Competing interests

The authors have declared no competing interests.

## Supplementary material

Supplementary material is available at *Genomics, Proteomics & Bioinformatics* online (https://doi.org/10.1093/gpbjnl/qzaxxxx).


## Acknowledgments

This research was supported by National Natural Science Foundation of China (Grant Nos. 32293252, 32341057, U19A2040, and 32273111), Natural Science Foundation of Hunan Province (Grant No. 2022JJ10035), Huxiang Young Talent Project of China (Grant No. 2021RC3093), National Key Research and Development Program of China (Grant No. 2023YFD2401602), Laboratory of Lingnan Modern Agriculture Project (Grant No. NT2021008), Special Funds for Construction of Innovative Provinces in Hunan Province (Grant No. 2021NK1010), Earmarked fund for China Agriculture Research System (Grant No. CARS-45), and 111 Project (Grant No. D20007). We extend our gratitude for the valuable assistance provided by English teacher Zhenzhen Dong in professional language editing.


## ORCID


0000-0003-4613-0380 (Li Ren)
0009-0003-5224-1738 (Mengxue Luo)
0000-0001-5901-8107 (Jialin Cui)
0000-0001-7162-4177 (Xin Gao)
0009-0001-7442-3079 (Hong Zhang)
0009-0004-6829-9800 (Ping Wu)
0000-0003-0688-1032 (Zehong Wei)
0009-0004-4525-5813 (Yakui Tai)
0009-0003-5896-7564 (Mengdan Li)
0000-0002-5735-1202 (Kaikun Luo)

0000-0001-5761-8571 (Shaojun Liu)

## References

[1] Mallet J. Hybrid speciation. Nature 2007;446:279–83.

[2] Degraeve S, De Baerdemaeker NJF, Ameye M, Leroux O, Haesaert GJW, Steppe K. Acoustic vulnerability, hydraulic capacitance, and xylem anatomy determine drought response of small grain cereals. Front Plant Sci 2021;12:599824.

[3] Paritosh K, Gupta V, Yadava SK, Singh P, Pradhan AK, Pental D. RNA-seq based SNPs for mapping in *Brassica juncea* (AABB): synteny analysis between the two constituent genomes A (from *B. rapa*) and B (from *B. nigra*) shows highly divergent gene block arrangement and unique block fragmentation patterns. BMC Genomics 2014;15:396.

[4] Qin Q, Wang Y, Wang J, Dai J, Xiao J, Hu F, et al. The autotetraploid fish derived from hybridization of *Carassius auratus* red var. (female) × *Megalobrama amblycephala* (male). Biol Reprod 2014;91:93.

[5] Liu S, Luo J, Chai J, Ren L, Zhou Y, Huang F, et al. Genomic incompatibilities in the diploid and tetraploid offspring of the goldfish × common carp cross. Proc Natl Acad Sci U S A 2016;113:1327–32.

[6] Hórreo JL, Ayllón F, Perez J, Beall E, Garcia-Vazquez E. Interspecific hybridization, a matter of pioneering? insights from Atlantic salmon and brown trout. J Hered 2011;102:237–42.

[7] Selz OM, Seehausen O. Interspecific hybridization can generate functional novelty in cichlid fish. Proc Biol Sci 2019;286:20191621.

[8] Luo J, Chai J, Wen Y, Tao M, Lin G, Liu X, et al. From asymmetrical to balanced genomic diversification during rediploidization: subgenomic evolution in allotetraploid fish. Sci Adv 2020;6:eaaz7677.

[9] Song C, Liu S, Xiao J, He W, Zhou Y, Qin Q, et al. Polyploid organisms. Sci China Life Sci 2012;55:301–11.

[10] Chen D, Zhang Q, Tang W, Huang Z, Wang G, Wang Y, et al. The evolutionary origin and domestication history of goldfish (*Carassius auratus*). Proc Natl Acad Sci U S A 2020;117:29775–85.

[11] Xu P, Zhang X, Wang X, Li J, Liu G, Kuang Y, et al. Genome sequence and genetic diversity of the common carp, *Cyprinus carpio*. Nat Genet 2014;46:1212–9.

[12] Zhang Y, Liu J, Fu W, Xu W, Zhang H, Chen S, et al. Comparative transcriptome and DNA methylation analyses of the molecular mechanisms underlying skin color variations in *Crucian carp* (*Carassius carassius* L.). BMC Genet 2017;18:95.

[13] Chen Z, Omori Y, Koren S, Shirokiya T, Kuroda T, Miyamoto A, et al. *De novo* assembly of the goldfish (*Carassius auratus*) genome and the evolution of genes after whole-genome duplication. Sci Adv 2019;5:eaav0547.

651 [14] Liu S, Liu Y, Zhou G, Zhang X, Luo C, Feng H, et al. The formation of tetraploid stocks of red
652 crucian carp × common carp hybrids as an effect of interspecific hybridization. Aquaculture
653 2001;192:171–86.

654 [15] Ren L, Gao X, Cui J, Zhang C, Dai H, Luo M, et al. Symmetric subgenomes and balanced
655 homoeolog expression stabilize the establishment of allopolyploidy in cyprinid fish. BMC Biol
656 2022;20:200.

657 [16] Ren L, Zhang X, Li J, Yan X, Gao X, Cui J, et al. Diverse transcriptional patterns of
658 homoeologous recombinant transcripts in triploid fish (Cyprinidae). Sci China Life Sci
659 2021;64:1491–501.

660 [17] Kemper KE, Visscher PM, Goddard ME. Genetic architecture of body size in mammals.
661 Genome Biol 2012;13:244.

662 [18] Visscher PM, Macgregor S, Benyamin B, Zhu G, Gordon S, Medland S, et al. Genome
663 partitioning of genetic variation for height from 11,214 sibling pairs. Am J Hum Genet
664 2007;81:1104–10.

665 [19] Romano C, Koot MB, Kogan I, Brayard A, Minikh AV, Brinkmann W, et al. Permian-Triassic
666 Osteichthyes (bony fishes): diversity dynamics and body size evolution. Biol Rev Camb Philos Soc
667 2016;91:106–47.

668 [20] Hochholdinger F, Baldauf JA. Heterosis in plants. Curr Biol 2018;28:R1089–92.

669 [21] Wu X, Li R, Li Q, Bao H, Wu C. Comparative transcriptome analysis among parental inbred and
670 crosses reveals the role of dominance gene expression in heterosis in *Drosophila melanogaster*. Sci
671 Rep 2016;6:21124.

672 [22] Maynard BT, Taylor RS, Kube PD, Cook MT, Elliott NG. Salmonid heterosis for resistance to
673 amoebic gill disease (AGD). Aquaculture 2016;451:106–12.

674 [23] Clasen JB, Norberg E, Madsen P, Pedersen J, Kargo M. Estimation of genetic parameters and
675 heterosis for longevity in crossbred Danish dairy cattle. J Dairy Sci 2017;100:6337–42.

676 [24] Shapira R, Levy T, Shaked S, Fridman E, David L. Extensive heterosis in growth of yeast
677 hybrids is explained by a combination of genetic models. Heredity 2014;113:316–26.

678 [25] Yang H, Li Q. The DNA methylation level is associated with the superior growth of the hybrid
679 crosses in the Pacific oyster *Crassostrea gigas*. Aquaculture 2022;547:737421.

680 [26] Ren L, Yan X, Cao L, Li J, Zhang X, Gao X, et al. Combined effects of dosage compensation
681 and incomplete dominance on gene expression in triploid cyprinids. DNA Res 2019;26:485–94.

682 [27] Springer NM, Stupar RM. Allelic variation and heterosis in maize: how do two halves make
683 more than a whole? Genome Res 2007;17:264–75.

684 [28] Pan FC, Bankaitis ED, Boyer D, Xu X, Van de Casteele M, Magnuson MA, et al. Spatiotemporal
685 patterns of multipotentiality in Ptf1a-expressing cells during pancreas organogenesis and
686 injury-induced facultative restoration. Development 2013;140:751–64.

687 [29] Xiong Y, Lei F. SLC2A12 of SLC2 gene family in bird provides functional compensation for the

688 loss of SLC2A4 gene in other vertebrates. Mol Biol Evol 2021;38:1276–91.

689 [30] Ren L, Zhang H, Luo M, Gao X, Cui J, Zhang X, et al. Heterosis of growth trait regulated by
690 DNA methylation and miRNA in allotriploid fish. Epigenetics Chromatin 2022;15:19.

691 [31] Li JT, Wang Q, Huang Yang MD, Li QS, Cui MS, Dong ZJ, et al. Parallel subgenome structure
692 and divergent expression evolution of allo-tetraploid common carp and goldfish. Nat Genet
693 2021;53:1493–503.

694 [32] Xu P, Xu J, Liu G, Chen L, Zhou Z, Peng W, et al. The allotetraploid origin and asymmetrical
695 genome evolution of the common carp *Cyprinus carpio*. Nat Commun 2019;10:4625.

696 [33] Wang J, Ye LH, Liu QZ, Peng LY, Liu W, Yi XG, et al. Rapid genomic DNA changes in
697 allotetraploid fish hybrids. Heredity (Edinb) 2015;114:601–9.

698 [34] Pastinen T. Genome-wide allele-specific analysis: insights into regulatory variation. Nat Rev
699 Genet 2010;11:533–8.

700 [35] Bao Y, Hu G, Grover CE, Conover J, Yuan D, Wendel JF. Unraveling *cis* and *trans* regulatory
701 evolution during cotton domestication. Nat Commun 2019;10:5399.

702 [36] He F, Wang W, Rutter WB, Jordan KW, Ren J, Taagen E, et al. Genomic variants affecting
703 homoeologous gene expression dosage contribute to agronomic trait variation in allopolyploid wheat.
704 Nat Commun 2022;13:826.

705 [37] Ren L, Li W, Qin Q, Dai H, Han F, Xiao J, et al. The subgenomes show asymmetric expression
706 of alleles in hybrid lineages of *Megalobrama amblycephala* × *Culter alburnus*. Genome Res
707 2019;29:1805–15.

708 [38] Pala I, Coelho MM, Schartl M. Dosage compensation by gene-copy silencing in a triploid hybrid
709 fish. Curr Biol 2008;18:1344–8.

710 [39] Rogers S, Macheda ML, Docherty SE, Carty MD, Henderson MA, Soeller WC, et al.
711 Identification of a novel glucose transporter-like protein-GLUT-12. Am J Physiol Endocrinol Metab
712 2002;282:E733–8.

713 [40] Xiao J, Kang X, Xie L, Qin Q, He Z, Hu F, et al. The fertility of the hybrid lineage derived from
714 female *Megalobrama amblycephala* × male *Culter alburnus*. Anim Reprod Sci 2014;151:61–70.

715 [41] Chen S, Zhou Y, Chen Y, Gu J. fastp: an ultra-fast all-in-one FASTQ preprocessor.
716 Bioinformatics 2018;34:i884–90.

717 [42] Rio DC, Ares M, Jr., Hannon GJ, Nilsen TW. Purification of RNA using TRIzol (TRI reagent).
718 Cold Spring Harb Protoc 2010;2010:pdb.prot5439.

719 [43] Patterson J, Carpenter EJ, Zhu Z, An D, Liang X, Geng C, et al. Impact of sequencing depth and
720 technology on *de novo* RNA-seq assembly. BMC Genomics 2019;20:604.

721 [44] Kim D, Paggi JM, Park C, Bennett C, Salzberg SL. Graph-based genome alignment and
722 genotyping with HISAT2 and HISAT-genotype. Nat Biotechnol 2019;37:907–15.

723 [45] Li H, Handsaker B, Wysoker A, Fennell T, Ruan J, Homer N, et al. The Sequence

724 Alignment/Map format and SAMtools. Bioinformatics 2009;25:2078–9.

725 [46] Srinivasan KA, Virdee SK, McArthur AG. Strandedness during cDNA synthesis, the stranded
726 parameter in htseq-count and analysis of RNA-seq data. Brief Funct Genomics 2020;19:339–42.

727 [47] Ren L, Cui J, Wang J, Tan H, Li W, Tang C, et al. Analyzing homoeolog expression provides
728 insights into the rediploidization event in gynogenetic hybrids of *Carassius auratus* red var. ×
729 *Cyprinus carpio*. Sci Rep 2017;7:13679.

730 [48] Song Q, Zhang T, Stelly DM, Chen ZJ. Epigenomic and functional analyses reveal roles of
731 epialleles in the loss of photoperiod sensitivity during domestication of allotetraploid cottons.
732 Genome Biol 2017;18:99.

733 [49] Krueger F, Andrews SR. Bismark: a flexible aligner and methylation caller for Bisulfite-seq
734 applications. Bioinformatics 2011;27:1571–2.

735 [50] Sun D, Xi Y, Rodriguez B, Park HJ, Tong P, Meong M, et al. MOABS: model based analysis of
736 bisulfite sequencing data. Genome Biol 2014;15:R38.

737 [51] Chen T, Chen X, Zhang S, Zhu J, Tang B, Wang A, et al. The Genome Sequence Archive Family:
738 toward explosive data growth and diverse data types. Genomics Proteomics Bioinformatics
739 2021;19:578–83.

# Figure legend

**Figure 1 Generation process, genotypes, and growth phenotypes in the six hybrid varieties derived from the intergeneric hybridization of goldfish and common carp**

**A.** The controlled genotypes of hybrid varieties obtained from the intergeneric hybridization of goldfish (*Carassius auratus* red var.), common carp (*Cyprinus carpio*), subsequent polyploidization, and interploid hybridization. **B.** Genotypes of the two interspecific hybrids (2nRC and 2nCR) and the four triploid varieties ($3nR_2C$, $3nCR_2$, $3nRC_2$, and $3nC_2R$) predicted based on the mapped reads of transcriptomes. **C.** Body weight in the six hybrid varieties (24 months after hatching). mtDNA, mitochondrial DNA.

**Figure 2 CNVs regulating allelic expression changes in the hybrid varieties**

**A.** Schematic diagrams of CNVs accompanied by hybridization, polyploidization, and interploid hybridization. White block represents the deletion of allele R or C. Gray box represents the duplication of allele R or C. **B.** Allelic CNV resulting from the ratio changes of alleles R *vs.* C. Here is the allelic CNV in the contiguous genes of chromosomes in four triploid individuals. For example, the loss of allele C was observed in the 92 contiguous genes of chromosome 19 (chr19). The 1:1 ratio of allelic copy number was observed in chr40 of $3nR_2C$-4 and in chr19, chr36, chr25, and chr31 of $3nRC_2$-2. In $3nR_2C$ and $3nCR_2$, red line represents $Log_{10}(2)$, while in $3nRC_2$, it is $Log_{10}(0.5)$. Dotted line represents the calibration line, which is used to determine whether CNV occurs. **C.** The changes in the expression ratio of alleles R *vs.* C (chr19, chr25, chr31, and chr36) accompanied by CNVs in $3nRC_2$-2. Green line represents the average values in the no-CNV and CNV regions. **D.** Individuals with no-CNV and CNV had significantly different expression ratios of alleles R *vs*. C (the chr19, chr25, chr31, and chr36 of $3nRC_2$-2) (two-sided *t*-test analysis). CNVs, copy number variations.

**Figure 3 Mitochondrial genetics regulating allele-specific expression in reciprocal hybrids**

**A.** Differential expressed analysis was performed in the diploid (2nRC and 2nCR) and triploid ($3nC_2R$ and $3nRC_2$) groups. "No DE" represents no differential expression. "High in R of 2nRC" represents the genes relating to higher expression in allele R of 2nRC than ones in 2nCR (1881 genes, green). There are also "High in R of 2nCR" (1393 genes, blue), "High in C of 2nRC" (1545 genes, yellow), and "High in C of 2nCR" (1697 genes, orange). The silencing of allele R was detected in the two genes (*bank1* and *ptf1a*) of 2nCR, while gene expression was observed in alleles of 2nRC. **B.** Schematic diagrams of nine allelic expression patterns regulated by mitochondrial genetics. Blue

represents the expression values in 2nCR and $3nRC_2$ (both mtDNA originating from both 2nCC), while red represents the expression values in 2nRC and $3nC_2R$ (both mtDNA originating from both 2nRR). "TPM in R" represents the expression values in allele R. FC, fold change; TPM, transcripts per million.

**Figure 4 Expression of 3693 growth-regulated genes altering body weight in the hybrid varieties**

**A.** PCC between the values of gene expression and body weight in the 3693 predicted growth-regulated genes. Among these genes, 3672 genes originated from subgenome R. Among them, the PCC values of 2032 genes are represented as blue dots and are greater than or equal to −0.5. Meanwhile, the PCC values of 1640 genes are represented as green dots and are less than −0.5. A gene (solute carrier family 2 member 12, abbreviated as *slc2a12*, black arrow) in subgenome C exhibited a negative correlation between gene expression and body weight (24 months after hatching). The other 20 genes in subgenome C showed positive correlations. **B.** Diversities in gene expression and body weight across the individuals of each variety. The SD of GPM values in the 3693 growth-regulated gene was performed to assess the expression diversity across individuals. The SD of body weight values was calculated to assess the growth diversity across individuals. **C.** A heatmap exhibiting the expression of the 21 growth-regulated genes in subgenome C across individuals. Two groups were classified into the six hybrid varieties based on the clustering of body weight and gene expression. PCC, Pearson correlation coefficient; GPM, gene per million; SD, standard deviation.

**Figure 5 Correlational analyses of expression of alleles R and C, allele-specific expression, and body weight**

**A.** Expression correlational analyses of the 3693 growth-regulated genes between the expression of AGPs and non-AGPs based on PCC values. **B.** Correlational analyses of the nine AGPs, which belong to the 21 growth-regulated genes in subgenome C. Blue represents the PCC between the expression of allele C and body weight. **C.** The distributions of PCC (violin plot) and body weight (box plot) values in the six hybrids. The median value of PCC is indicated in figure. **D.** A two-sided *t*-test of PCC values was performed to detect the effects of gene regulatory networks between two hybrid varieties. **E.** The distribution of genes with $|PCC| > 0.5$. For example, 194 genes were shared among the six hybrid varieties (red). AGPs, allelic gene pairs;

**Figure 6 Analyses on DNA methylation, allele-specific expression, and histological**

**observation between hybrids with different body weights**

**A.** DNA methylation levels of different gene elements in the two triploids ($3nR_2C$ and $3nC_2R$) and their inbred diploid parents (2nRR and 2nCC). Each region was divided into twenty bins based on its total length. The methylation ratio of subgenome R was higher in two triploids than in 2nRR, while the methylation ratio of subgenome C was higher in $3nR_2C$ than in $3nC_2R$ and 2nCC. "$3nR_2C$" represents the combined methylation ratios of subgenomes R and C in $3nR_2C$. "$3nR_2C$-R" represents the methylation ratios in the subgenome R of $3nR_2C$**. B.** DNA methylation level of the 2094 growth-regulated genes. **C.** The expression levels of the 2094 growth-regulated genes. **D.** Cross-section of skeletal muscle (H&E staining) showing the myofibers of the two triploids and their inbred parents (2nRR and 2nCC) (n = 3 biologically independent samples). Scale bar = 100 μm (10X). H&E. hematoxylin and eosins.

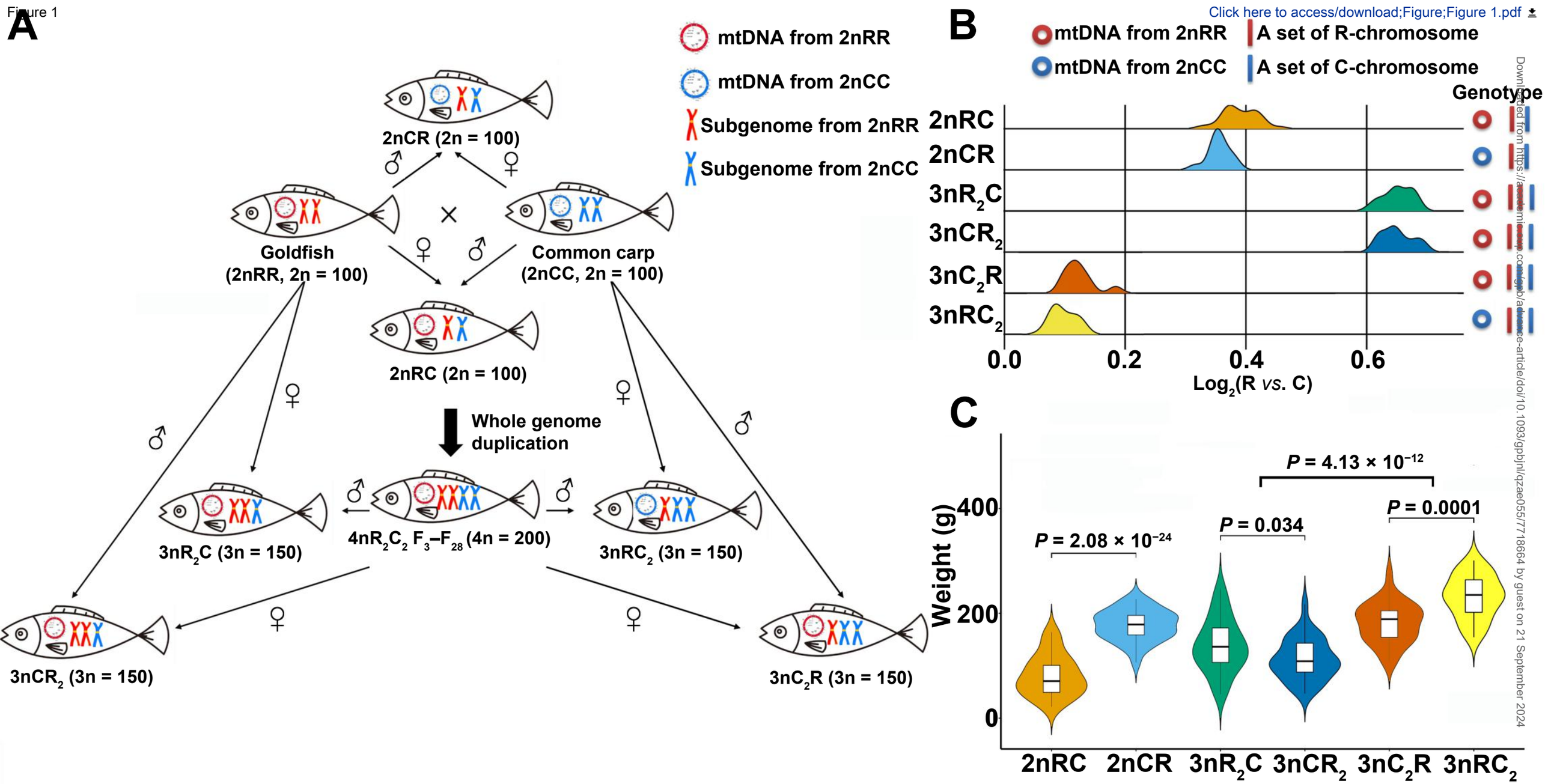

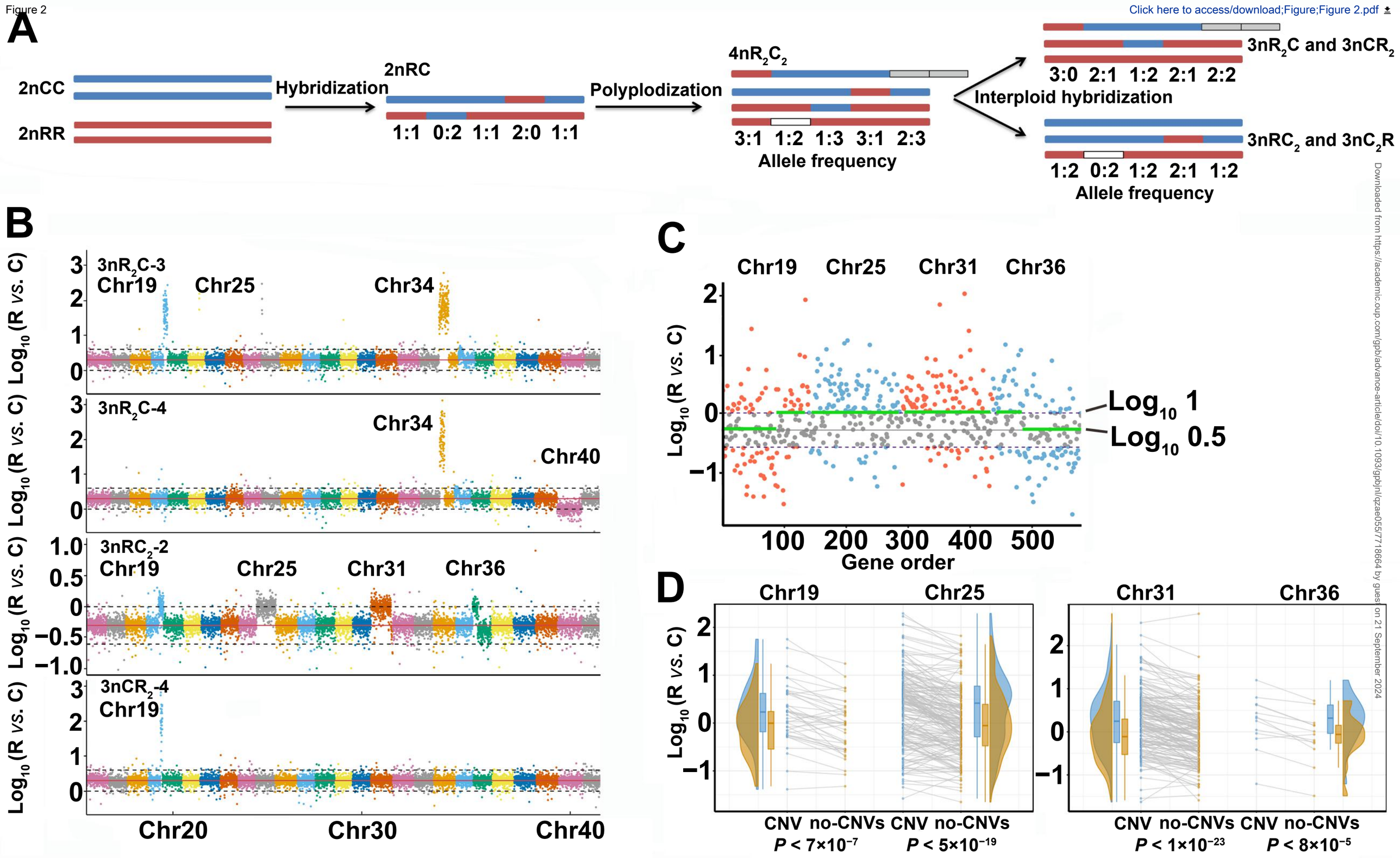

A

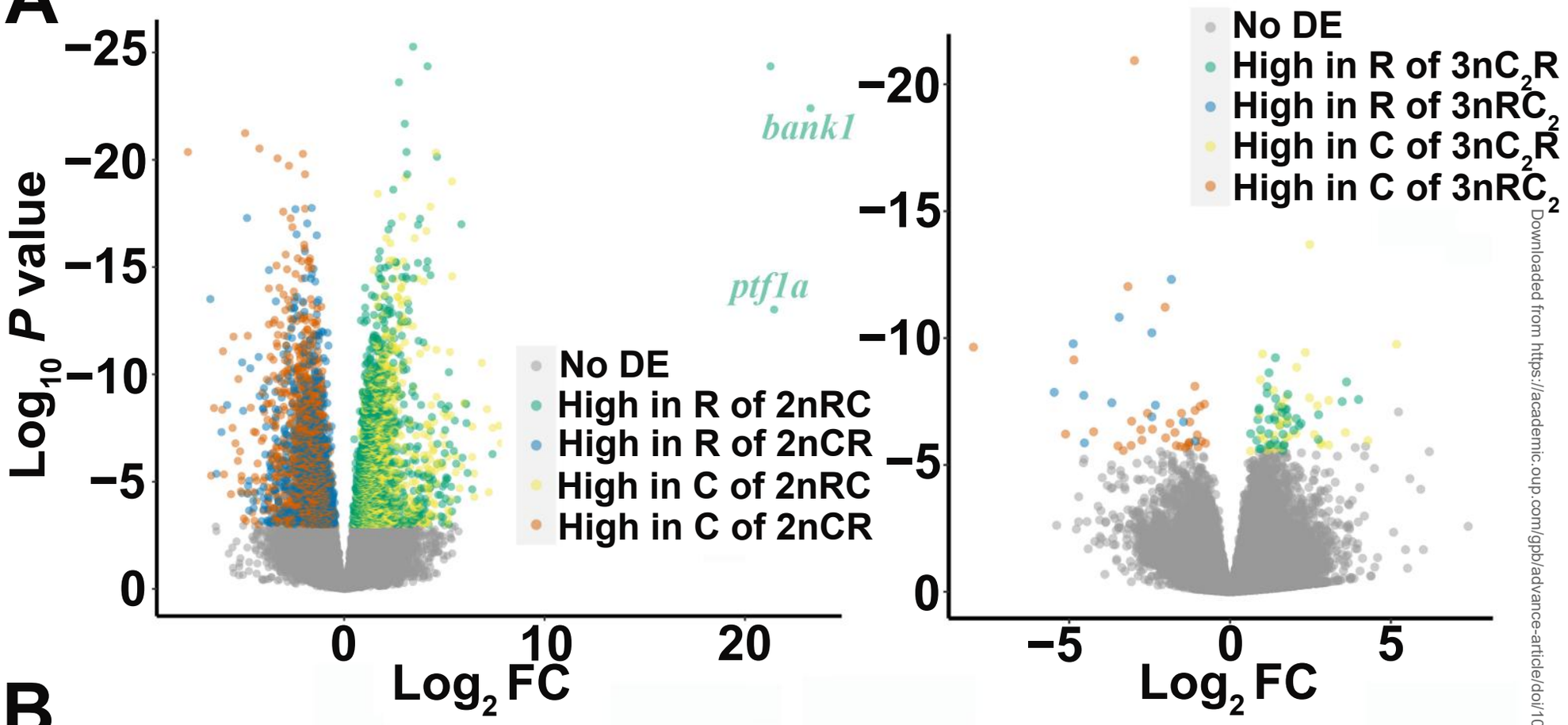


B

| TPM in R TPM in C | Diploid | Triploid | TPM in R TPM in C | Diploid | Triploid |
|---|---|---|---|---|---|
| I | 5 | 0 | VI | 507 | 13 |
| II | 479 | 5 | VII | 10 | 0 |
| III | 261 | 0 | VIII | 767 | 23 |
| IV | 414 | 11 | IX | 311 | 0 |
| V | 15,265 | 17,962 | | | |

Figure 4